Desalination and Water Treatment
www.deswater.com

doi: 10.5004/dwt.2023.29912

307 (2023) 232–250
September

Hydrodynamics and heat transfer characteristics of bio-synthesized SiC-alkaline water and ZnO-alkaline water nanofluids in an aluminum plate pin-fin heat sink

V. Rajangam[a], N. Anbuchezhian[b], R. Ashok Kumar[b], P. Renugadevi[c], M. Anish[d,*]

[a]*Department of Mechanical Engineering, Panimalar Engineering College, Chennai, India, email: rajangam.accet@gmail.com*
[b]*Department of Mechanical Engineering, R.M.D. Engineering College, Chennai, India, emails: anbunpd@gmail.com (N. Anbuchezhian), ashok.kumar19872003@gmail.com (R. Ashok Kumar)*
[c]*Department of Computer Science and Engineering, VIT University, Chennai, India, email: renugadevi.2020@vitstudent.ac.in*
[d]*School of Mechanical Engineering, Sathyabama Institute of Science and Technology, Jeppiar Nagar Chennai, India, email: anish.mech@sathyabama.ac.in*

Received 29 March 2023; Accepted 22 August 2023

ABSTRACT

The hydrodynamic and thermal performance of a heat sink constructed of an aluminum plate with pin-finned fins is investigated in this study utilizing two nanofluids, SiC-alkaline water and ZnO-alkaline water. The heat sink core plate, which is used to cool electronic equipment, must have the following dimensions: 12 mm (length) × 40 mm (width) × 40 mm (length) (H). It is shielded from the weather by being contained in an aluminum plexiglass container that is insulated from the outside world with insulator foam. As a result, the heat sink's bottom surface gets a continuous heat flow of 118.9 kW/m^2, while the nanofluid is pumped through it at the same constant input temperature. Following that, the thermal performance of the heat sink is evaluated. The nanofluids are generated at volume concentrations of 0.25%, 0.5%, 1.25%, and 2% with water serving as the foundation fluid, and their performance is evaluated. The heat sink's hydrodynamic performance was evaluated by comparing the pressure differential between the entry and exit sites to a reference pressure. According to the study, when SiC-alkaline water nanofluids were added to water at a rate of 2%, pumping power increased by 17% and 33%, respectively. Following the testing, the average heat transfer coefficients of the nanofluids under consideration increased by 18% and 16%, respectively, and decreased by 14% and 12%.

Keywords: Plate pin-fin heat sink; Nanofluids; Heat transfer coefficient; Thermal resistance; Pumping power; Alkaline water

1. Introduction

The incredible technological advances that have been made in the past 10 y, which have made it possible to build transistors with dimensions on the nanometer scale and implement these transistors in electronic chips, are among the most significant achievements that humans have made in this time period. This is because the ability to build transistors with dimensions on the nanometer scale has made it possible to build electronic chips with dimensions on the nanometer scale. Researchers have, for a very long time, regarded the flow of heat that is created by such electronic devices as a serious difficulty, both in terms of the technique that is used to remove it and the way that it is produced in the first place. In view of the fact that traditional heat dampers are unable to remove a heat flow of this scale, the development of novel techniques and technologies seems to be an essential need in the environment in which

* Corresponding author.

this issue is being discussed. Given the context in which it is being studied here, an aluminum plate pin-finned heat sink with a high surface area to volume ratio seems to be an adequate device for removing the heat flow that is in question. This is because the ratio of surface area to volume is high. In the past, one of the primary research foci has been on developing methods for producing turbulence in fluid flow, with the end goal being to increase the amount of heat that can be transferred by convection inside the heat sink. The end result of this research has been to increase the amount of heat that can be transferred.

Researchers are interested in the use of nanofluid as a cooling fluid because it has the potential to increase the convective heat transfer coefficient and create an almost constant temperature across the heat sink. The idea that nanofluid may be used as a cooling fluid has also piqued the interest of scientists. It is essential to evaluate the applicability of utilizing nanofluids in teeny thermal convection devices, which is something that is currently being investigated, in order to continue debating and researching the hydrodynamic and thermal performance of nanofluids. This is something that is currently taking place. At the moment, investigations on this topic are being carried out. This will spark more conversations and inquiries on the topic at hand. The recently made discovery of nanofluid [1] is anticipated to result in a significant enhancement to the efficiency of the newly developed liquid coolant. A nanofluid is a suspension of nanoscaled particles in a base fluid that is retained at a nanoscale distance between the particles. The particle sizes of a nanofluid may range from 10 to 100 nm. Particles in the suspension have sizes that range anywhere from 10 to 100 nm. The word "nanofluid" refers to a fluid in which individual particles have nanoscale gaps between them while they are suspended. When solid particles are mixed with liquids, the liquid's thermal conductivity increases because the higher thermal conductivity of the solid particles is transferred into the liquid and increases the liquid's own thermal conductivity. These events occur due to the fact that solid particles are able to carry heat more effectively than liquids can. Reducing the size of the heat sink is another way that may be used to improve the capacity of a system to remove heat in an efficient manner [2–5]. Because of this, the machine is in a position to extract more heat from its surroundings than it would have been able to do in any other circumstance. The performance of nanofluids when applied to nanoscale heat sinks for the purpose of cooling electronic components has been the subject of a significant amount of theoretical, analytical, and even some practical research over the past two decades [6–8]. This research aims to better understand how nanofluids can be used to effectively cool electronic components. These examinations have been carried out with a wide array of diverse approaches each with their own distinct advantages.

Chandra Sekhara Reddy and Vasudeva Rao et al. [9] produced three different nanofluids. Each nanofluid was evaluated in vitro to see whether or not it was effective, and the results showed that all three were successful. Nanofluids were created by combining a broad range of various combinations of ethylene glycol and water with nanoparticles of titanium dioxide. They were characterized by looking at the thermal conductivity of a solution as a function of temperature in addition to the concentration of nanoparticles in a certain volume of solution. This was done in order to determine the properties of the nanoparticles. According to the results of the research, an increase in temperature led to an increase in the thermal conductivity of TiO_2 nanofluids. This rise was also accompanied by an increase in the volume concentration of TiO_2, which contributed to the overall increase. Yiamsawasd et al. [10] investigated the impact that temperature and volume concentration had on the conductivity of water-based and water-ethylene glycol-based Al_2O_3 and TiO_2 nanofluids, respectively. The nanofluids were tested for conductivity at a range of concentrations, from 0% to 100% by volume. Al_2O_3 and TiO_2 served as the primary components of each of these nanofluids. In order to carry out the comparison, we used both the data that we collected from our experiments and the models that we found while doing our inquiry. Both of these were utilized together. According to the findings, there was a relationship between the relative volume concentration and an increase in the nanofluid conductivity of Al_2O_3 and TiO_2 of between 5% to 30% and 2% to 20%, respectively, when the concentration was between 1% and 8%. This was the case when the concentration was between 1% and 8%. This was shown to be the case upon doing an analysis of the data. Keblinski et al. [11] looked at how heat is transported via the use of nanofluids. The researchers came to the conclusion throughout the course of their examination that the creation of a layer of liquid cluster surrounding a nanoparticle has a major influence on the thermal conductivity of nanofluids. This was one of the main findings of the analysis. During the course of the experiment, it was found out that the Brownian motion of the nanofluid did not have a substantial influence on the augmentation of the heat transmission capabilities of the nanofluid. This was determined as a result of the findings of the previous sentence. Mat Tokit et al. [12] found that Brownian motion plays an essential function in increasing thermal conductivity. They found that it does this by encouraging the formation of nanoparticle clusters at a lower velocity than the velocity of the particle itself. Because of this, the thermal conductivity of the material exhibits increased levels. Naphon and Nakharintr [13] looked into the impact that the temperature of the nanofluid intake, the Reynolds number of the nanofluid, and the heat flux had on the ability of TiO_2-deionized water nanofluids to transmit heat. It was shown that the average heat transfer rates were greater when nanofluids were used as a coolant rather than deionized water in the same capacity. This was the case for the cooling system. We were able to do much more by switching out the Al_2O_3-water nanofluid coolant that was contained inside a copper minichannel heat sink for pure water. Ho and Chen [14] investigated how effectively using forced convection to transport heat around in a heat sink might be accomplished. A copper minichannel heat sink served as the primary component of the system, and its design prioritized making optimum use of available space. The nanofluid composed of Al_2O_3 and water that served as its secondary component and operated as a chiller. According to the findings, a heat sink cooled with nanofluid performed far better than a heat sink cooled with water in each and every test that was done on the device. The heat sink that was cooled using nanofluids performed noticeably better than the heat

sink that was cooled using water in terms of average heat transfer coefficients, thermal resistance, and wall temperature, as well as in terms of both of these metrics. According to what they found, the efficacy of the heat transfer achieved by using the nanofluid in the heat sink was also examined in relation to the pumping power penalty associated with its utilization, and the findings were favorable.

Das et al. [15] conducted research to determine how temperature affects the ability of nanofluids to transport heat and came up with some intriguing conclusions from their investigation. They found that the thermal conductivity increased from 14% to 36%, respectively, as the temperature increased from 21°C to 51°C when they used a concentration of CuO-H_2O that was 4% in volume, and when they increased the temperature from 21°C to 51°C. In an experimental study Nguyen et al. [16] investigated the enhancement of the heat transfer coefficient of Al_2O_3-H_2O nanofluid compared to the heat transfer coefficient of pure water. It was possible to increase the heat transfer coefficient by 40% by using 6.8% volume of nanoparticles. Nanoparticles with smaller particle sizes outperformed particles with larger particle sizes in terms of thermal performance. Inside the framework of their study Selvakumar et al. [17] investigated the potential effects that the presence of an Al_2O_3-H_2O nanofluid may have on the pace at which heat is transferred within a conventional water block. According to the findings of the researchers, a nanofluid containing 20–30 nm of alumina has a conductivity that is about 20% greater than that of deionized water. It has been shown that the use of nanofluids results in a little decrease in the amount of pumping power required. Whelan et al. [18] designed, constructed, and researched a tube array remote heat exchanger for the purpose of cooling CPUs. They were successful in maintaining a temperature that was tolerable at the base while also reducing the amount of thermal resistance. Ijam et al. [19] studied the thermal conductivity, heat transfer, and pumping power of Al_2O_3-water and TiO_2-water nanofluids in a laminar flow for a copper microchannel heat sink. They did this by using a copper microchannel heat sink. Researchers found that the thermal conductivity of water was increased by 11.98% when Al_2O_3 nanoparticles were added at a volume percentage of 4%. This was one of the findings of their investigation. Tullius and Bayazitoglu [20] conducted research on the effect of an Al_2O_3-H_2O nanofluid on the effective thermal conductivity of a minichannel heat sink that had a circular fin structure. This research was carried out with the use of a minichannel heat sink. The heat transmission properties of the nanofluid have been significantly enhanced as a result of recent research and development. As a result of nanoparticle deposition, an issue with a tiny surface defect was observed, which was responsible for the reduction in heat transfer performance. In a recent study, Harish Kumar et al. [21] examined the impact of CuO-water nanofluid fractions of 0.1% and 0.2% on the efficiency of a copper heat sink with a narrow channel under conditions of continuous heat flow. They discovered that when both the volume flow rate and the nanoparticle volume percentage of the nanoparticles under research rose, the convective heat transfer coefficient also increased. The convective heat transfer coefficient rose as a result of both of these causes. The study's conclusions show that when compared to the performance of deionized water with a nanofluid volume fraction of 0.2%, the pumping power improves by 15.11%. Overall, there is an increase of 15.11% as a consequence. The largest drop in interface temperature, which was reported to be 1.15°C, was seen for the nanofluid with a volume percentage of 0.2%. The biggest increase in convective heat transfer coefficient, which was reported to be 29.63%, was also discovered in the nanofluid with a volume percentage of 0.2%. These two discoveries were made simultaneously.

In spite of the fact that the plate fin heat sink (PFHS) offers a number of benefits, such as the simplicity of machining, the ease of construction, and the low cost, there is a fundamental flaw in the arrangement of the PFHS that needs to be fixed. This flaw is that the PFHS does not have enough space between its individual fins. According to Yu et al. [22], the smoother flow of fluid that is passing through the heat exchanger is desired when trying to boost the heat transfer performance of the heat exchanger. This is because the parallel plate fins make the flow of fluid smoother. It was recommended that a plate pin-fin heat sink, also known as a PPFHS, be used to adjust the structure of a PFHS in order to change the turbulent character of the flow within the heat sink. This was done in order to vary the temperature of the fluid that was moving through the heat sink. In addition to that, the performance of the heat transmission would be significantly increased. The PPFHS was created by combining a PFHS with a few pins that were put between the plate fins of the PFHS. This allowed for the construction of the PPFHS. Yang and Peng [23] carried out research with the purpose of determining how the functionality of the system will be impacted by a number of different pin-fin configurations. The results of the researchers indicate that the plate-circular pin-fin heat sink outperforms the PFHS when it comes to the overall performance of the two types of heat sinks. Heat transmission and pressure drop were analyzed for both inline and staggered pin-fin arrays in Sparrow et al. [24]. According to the findings of the researchers, the heat transfer coefficient of the staggered array is greater than that of the inline array, despite the staggered array having a larger pressure drop. Soodphakdee et al. [25] looked at a heat sink using the conventional fin shapes used in the industry (round, elliptical, and square). Elliptical fins perform well even in conditions of minimal pressure drop and pumping power. The production of CeO_2 tiny chemicals from the cannabis indica plant utilizes biosynthetic technology, which is less hazardous and more suitable with conventional chemical procedures [26,27]. Chemical processes can be replaced by the straightforward, incredibly efficient, and beneficial to the environment biosynthetic approach [28]. TiO_2 NP treatments outperformed controls in terms of seed germination, root development, and plant growth [29].

Although there are several computational models of heat sinks for use in electronic circuit cooling that make use of nanofluids, relatively little real research is being conducted in this field at this time. As a direct consequence of this, the research phase of the project got underway. The current study explores the performance of a plate pin-finned heat sink that has three pins in each channel. This heat sink has three channels. The flow entering the channel from one side and then moving through the elliptical pins is what causes

the turbulence that is created by this heat sink [30,31]. Even though it has a higher convective heat transfer coefficient than laminar flow does, turbulent flow showed outstanding thermal performance. This is because laminar flow has a smaller convective heat transfer coefficient. This study also looked at two other nanofluids, namely SiC-alkaline water and ZnO-alkaline water. Both of these nanofluids have the potential to be beneficial in the not-too-distant future for the construction of tiny pin-finned heat sinks, in addition to other nanofluids. The purpose of this study was to evaluate the effects of volume concentration and Reynolds number on the convective heat transfer coefficient, thermal resistivity, Nusselt number, and pumping power.

2. Procedures and setup for experiment

A calibrated rotameter is used to measure the flow rate. A data collection system, pressure drop detecting equipment, and a heat sink test section are all part of the test loop. A closed loop cooling nanofluids system would typically contain a pump, storage tank, flow rate sensor, and ball valve that could be used to modify the flow rate. Installing a thermal bath before to the pump allows you to regulate the temperature of the water entering the heat sink while the pump is operating. To monitor the average temperature of the nanofluids flowing through the manifold, two K type thermocouples with an accuracy of 49.1°C were inserted at the device's input and output. To effectively gather and monitor all temperature values, you will need to use not one, but two Testo 779 data loggers. The ability to connect data loggers to computer systems through USB connections provides the ability to gather and store data. For all calibrated thermocouples, the temperature range for which they may be utilized is 0°C–100°C. To complete its life cycle, it must pass through the PPFHS after being pumped out of the storage tank. A ball valve may be utilized to control the flow rate of the cooling nanofluid. One of the test section's components is an isolated heater placed inside a concrete block. There are additional insulating plexiglass cover plates, a tiny plate with a pin-finned heat sink, and a pin-finned heat sink in the test area. Fig. 1 a schematic illustration of the test section, depicts a test section that serves as an example of the test section. Table 1 outlines the geometrical properties of plexiglass cover plates.

2.1. The PPFHS

A computer numerical control (CNC) machine was used in the process of fabricating the heat sink, which consisted of a square block composed of aluminum. The width, at 40 mm, is the most critical dimension, followed by the length, at 40 mm, and the height, at 12 mm. Within each channel of the heat sink, there are three pins with an elliptical cross-section that have been threaded through them. On four different K-type thermocouples, an accurate temperature reading of 49.1°C was achieved by using a mixture that was both thermally conductive and comprised of copper powder and silicon paste. In order to fit the thermocouples, holes measuring

Table 1
Typical plexiglass dimensions and shapes (dimensions are in millimeters)

L_p	200
W_p	50
D_h	7.375
H_p	10
l_{h1}	20
l_{h2}	70
W_h	25
t_1	10
t_2	5
t_3	4

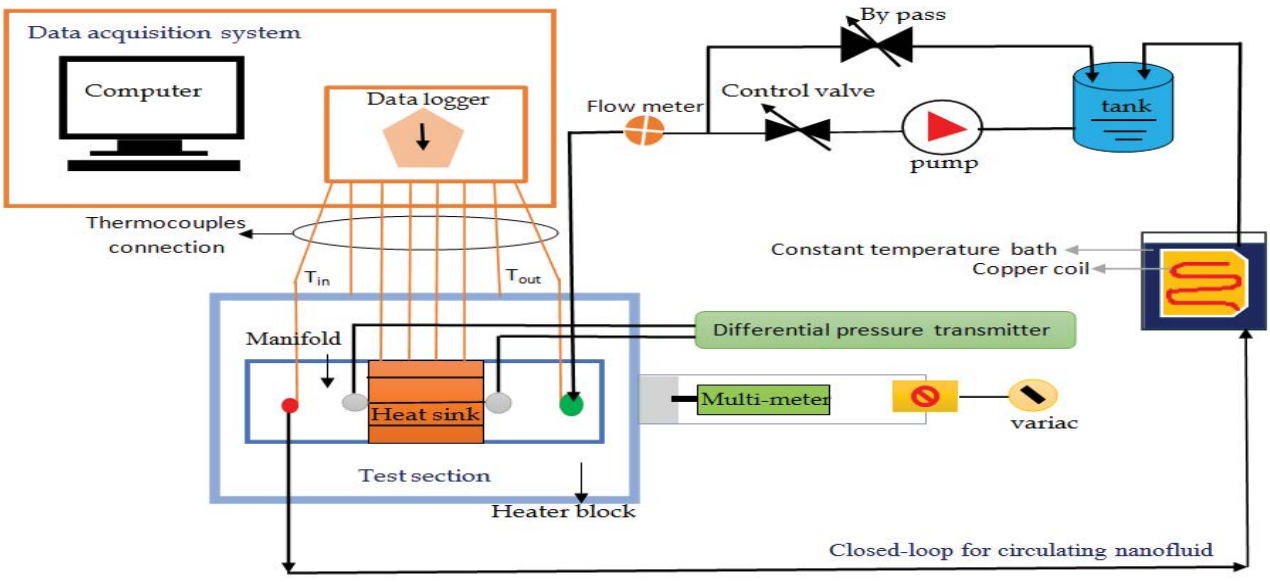

Fig. 1. Experiment set-up.

20 mm in depth and 1.0 mm in diameter were drilled. Before it enters the central channel, the temperature of the heat sink's base is measured at four different locations before it is averaged. They are 7, 17, 27, or 37 mm away from the front of the heat sink, depending on where they are positioned around the perimeter of the heat sink. Fig. 2 illustrates the geometrical characteristics of the heat sink, which include the following elements: The heat transfer surface area (HSA) is 0.001922 m^2 and the pin height is 12 mm.

2.2. Inlet and outlet chambers

In order to prevent heat from the surrounding environment from being transferred to the thing being tested, the ultimate heat sink is enclosed in a plexiglass cage. Even while this causes some heat to be lost, the end outcome is not significantly altered as a direct consequence of this. Styrofoam is used to insulate all of the plexiglass box's surfaces, with the exception of the bottom of the heat sink, which is made of metal. In order to improve the effectiveness of the heat transfer between the base of the heat sink and the heater block, silicon paste is often used.

2.3. Heater block

In order to simulate the mechanism by which heat is accumulated within an electronic chip, a heater block maintains a consistent flow of heat to the base of the heat sink. The dimensions and shape of the heater block are shown in Fig. 3. Due to the fact that the fiberboard enclosure was packed with slag wool, there was no way for heat to go through the box other than at the point of direct contact that existed between the heater block and the heat sink. Six thermocouples of the K type are used to measure the heat flux emitted by the cylinder-shaped heater block. Every one of the holes is exactly three centimeters deep, with the exception of the very first one.

2.4. Data acquisition and pressure measuring unit

In order to accomplish this goal, two thermocouples of the K type with a precision of 0.18°C each were installed at the intake and exit of the manifold. The temperature of the heat sink's bottom surface will be measured to an accuracy of 0.18°C using four thermocouples of the K type. Thermocouples with 1 and 20 mm diameter were put into the heat sink 230 at a distance of 1 mm from the bottom. In order to measure the heat flux generated by the heater

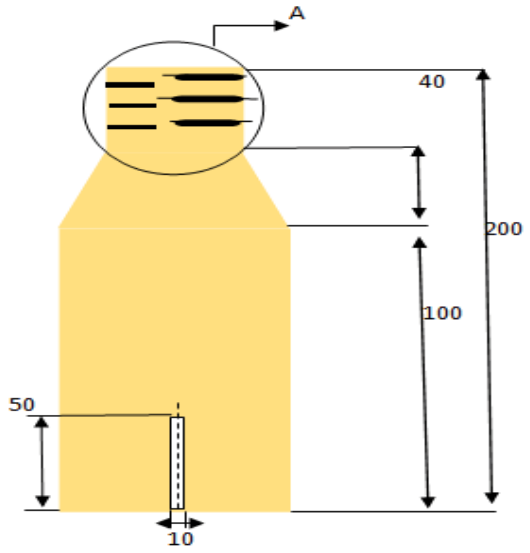

Fig. 3. Geometric configuration of heater.

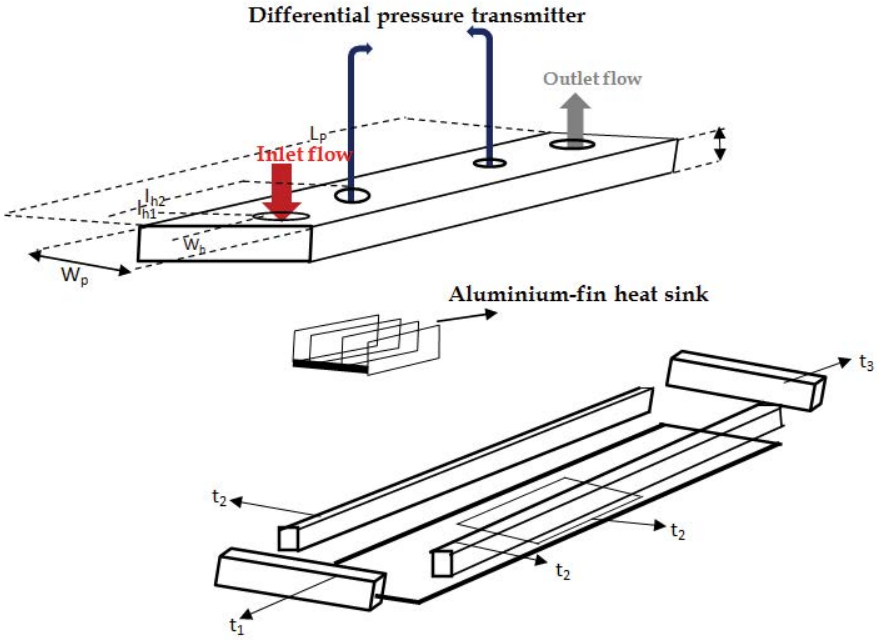

Fig. 2. Schematic of the test section.

block, six thermocouples of the K type will be used. The heater block will have six thermocouples of the K type put in it so that it can be used to measure the amount of heat flux that is generated by the heater block. Putting the thermocouple sensors and the data logger in communication with one another. The temperature will be recorded continuously for the whole of the experiment. The fact that there has been no change in temperature suggests that the current temperature is maintaining itself at 235. It is linked to a USB port on the personal computer. Calibration is performed on thermocouples ranging from 0°C to 100°C. These high-precision differential pressure transmitters were able to monitor the pressure drop of fluid that was passing through the heat sink to within 1.0 Pa of accuracy [32].

3. Nanofluid preparation and characterization

We often consider excessive energy consumption, low purity, uneven particle size distribution, enormous amounts of secondary waste, and long-term environmental effects when we think about physical processes. Chemical processes have several advantages, including low energy consumption, consistency of particle size, low cost, and little environmental effect. Anbuvannan et al. [33] claim that as the need for environmental protection has grown, so has the usage of zinc oxide. Microorganisms, plant extracts, and plant enzymes are all used in the chemical reactions of green synthesis. Peels, flowers, fruits, seeds, leaves, peels, and roots are just a few examples of the many plant parts that might regulate and reduce ZnO production. ZnO may be lowered and stabilized with the use of these extracts more successfully. Vijayakumar et al. [34] investigated plant extracts to see whether they might be utilized to produce zinc oxide, which is more potent against a larger variety of bacteria when produced chemically. If these compounds are to be employed, non-toxic, mild chemicals must be applied to people. In the future, it's possible that plant extracts will be used to create green zinc oxide, which is ecologically benign. This technique allows the production of nanoparticles from Hibiscus rosa-sinensis leaf extracts. 15 min at 70°C while stirring a 50 mL amount of leaf extract. The solution needed 5 g of zinc nitrate added to it due to the high temperature. A yellow paste is added after the mixture has been cooked. The paste was gathered in a ceramic crucible and fired in a furnace for 2 h to 400°C. After the procedure, fine white powder may be gathered and used for a variety of things. Zinc oxide nanoparticles that have been chemically produced and then purified to a 99.9% purity are used to create nanofluids. The creation of these particles involves the use of cetyltrimethylammonium bromide (CTAB) as a surfactant. The steps below should be followed to create nanofluids: To get the best results, use an ultrasonic granulator for 30 min after diluting the solution with water. To achieve the required amplitude, the ultrasonic vibrator's setting has been changed to 0.6 on the scale. This component causes vibrations in ZnO nanoparticles. The nanometer-sized particles can be seen quite clearly in the SEM picture shown in Figs. 2 and 3.

3.1. Chemical synthesis of zinc oxide nanoparticles

In the beginning, natural zinc acetate is used. Caustic soda at a concentration of 2 M was added to newly agitated zinc acetate after it had been well mixed with intelligence using 1 M zinc acetate. After that, the zinc acetate was mixed well. As a result of the decision to employ white slurry, a significant quantity of white precipitate suspension was produced and agitated for a period of 18 h. This contributed to a more even distribution of the precipitation. A muffle chamber was used to filter and cleanse the material before it was put through a calcination process at 400°C. When the temperature reaches 400°C, the particles begin to dissolve and turn into a black ash.

3.2. Biological synthesis of zinc oxide nanoparticles

In this method, nanoparticles are produced by using extracts from the leaves of the *Hibiscus rosa-sinensis* plant. These nanoparticles have a wide range of potential applications. In preparation for the experiment, a leaf extract of 50 mL was heated in a stirrer for 15 min at a temperature of 70°C. In order to make the solution effective at high temperatures, 5 g of zinc nitrate were added to it just before it was used. A yellowish paste is placed before to the cooking process. In order to do this, the paste needs to be heated for 2 h at a temperature of 400°C in a furnace. A crucible made of ceramic that is used to accumulate paste. A white powder is the result of the reaction. Following the processing, this powder may be used in a variety of contexts.

3.3. Chemical synthesis of silicon carbide nanoparticles

Silicon tetra chloride was used here as the foundational substance. The next move has already been deliberated about. When added 200 mL of cold water, the addition of distilled water caused the temperature to drop below zero. In order to draw a conclusion from the experiment, the cold beaker is brought up to the standard room temperature. A homogenous solution was achieved by stirring the contents of a beaker with a magnetic stirrer for a period of half an hour. Up until the nanoparticle extraction process is finished, the temperature of the bath will remain constant at 150°C. The operation will be carried for a second time when the bath has been cooled to 100°C.

3.4. Biological synthesis of silicon carbide nanoparticles

Moringa oleifera leaf extracts are used to make nanoparticles. The leaves must be picked, cleaned, and sun-dried for 7 d before usage. The fragments were then crushed into powder. 10 g of powder and 100 mL of ethanol to form a drink and 1 h at 500°C. The mixture becomes ethanolic leaf extract when filtered using Whatman paper (ethanolic leaf extract). After heating to 50°C, 0.5 M silicon tetraisopropoxide was added.

The nanofluids are created by the use of a two-stage technique. The nanoparticle will be created initially, and then spread throughout the basic fluid. The goal of this strategy is to achieve this goal. If the current research is any indication, this process will result in the development of a stable and homogeneous nanofluid. In these studies, silicon and zinc dioxide were utilized, which resulted in particles with smaller diameters than silicon and zinc dioxide, namely 10, 20 and 45 nm, respectively. To accomplish the desired results,

it is also possible to utilize distilled water to attain the maximum degree of purity. Table 2 summarizes the thermophysical properties that water and nanoparticles share.

The nanoparticle concentrations used in the studies were 0.5%, 1%, 1.5%, and 2% of the total volume of the sample. Volume concentration was attempted by weighing nanoparticles and adding them to a basic fluid composed of three distinct phases of water. This was done to get the intended outcome. Sonication was done for 30 min on each of the three phases of the procedure at each step of the method. To do this, an ultrasonic homogenizer, namely a UP 400S type, is used to homogenize the mixture. This equipment, with a power output of 400 W and a frequency of 24 kHz, is utilized to attain the required level of uniformity. As a result of this action, the aggregation of nanoparticles in the base fluid is decreased, and the creation of a homogenous mixture is achieved. Two nanofluids will be produced at the end of the operation. These nanofluids will be made up of SiC-alkaline water and ZnO-alkaline water. These nanofluids, which include a number of elements, each have one of four distinct volume concentrations of those elements. Scientists most often utilize nanoparticles of SiC and ZnO, both of which are zinc oxides, in the process of performing experimental research. A number of researchers have investigated the thermophysical properties of nanofluids composed of SiC-alkaline water and, as well as nanofluids composed of ZnO and alkaline water in recent years. These thermophysical qualities include heat transfer [35], thermal conductivity [36], and viscosity [37]. Nanofluid research is required because nanoscale fluids have the potential to be used in a wide variety of applications, including the control of welding equipment and the cooling of engine components in vehicles. Because of this potential, it is critical that research on nanofluids be done. They can also cool high-heat flux devices, such as high-power microwave tubes and laser diode arrays, which can be used in high-power laser diode arrays, allowing them to function at lower temperatures. This would enable the gadgets to function better. As a result, high-power laser diode arrays may function at a greater efficiency.

3.5. Thermophysical properties of nanofluids

It is essential to determine the thermal conductivity of nanofluids right from the start in order to ensure that theoretical and experimental results are in agreement with one another [38]. The H-C model may be used to make predictions about the thermophysical properties of nanofluids. This approach is used rather often for calculating the thermal conductivity of fluids.

Table 2
Input and exit temperatures, flow rates, heat fluxes to the base, and laboratory air temperature

Nanofluid	SiC – AW	ZnO – AW
Inlet temperature (°C)	50	50
Outlet temperature (°C)	51.0–54.9	50.8–54.6
Volume flow rate (m^3/s) × 10^{-6}	8.34–27.4	8.21–33.9
Heat flux to the base (W/m^2) × 10^6	0.145	0.145
Air temperature (°C)	22.0	22.0

$$k_{\mathrm{nf}} = \left[\frac{k_p + (m-1)k_t - (m-1)\varnothing(k_t - k_p)}{k_p + (m-1)k_t + \varnothing(k_t - k_p)}\right]k_t \tag{1}$$

For the purpose of computing the thermal conductivity of spherical particles, it is possible to make use of both the empirical form factor N and the sphericity of the particles. When determining whether or not anything has a spherical shape, it is essential to keep this in mind as one of the determining factors. The symbol for the thermal conductivity of nanoparticles is denoted by the letter k_{nf}, while the letter k_p is used to denote the thermal conductivity of base fluids. Previous investigation on the thermal conductivity of nanofluids was carried out by Murshed et al. [32], but Bruggeman created the mathematical model that is described in the following sentence:

$$k_{\mathrm{nf}} = 0.25\left[(3\varnothing - 1)k_p + (2 - 3\varnothing)k_t\right] + \frac{k_t}{4}\sqrt{\Delta} \tag{2}$$

$$\Delta = \left[(3\varnothing - 1)^2\left(\frac{k_p}{k_t}\right)^2 + (2 - 3\varnothing)^2 + 2\left(2 + 9\varnothing - 9\varnothing^2\right)\left(\frac{k_p}{k_t}\right)\right] \tag{3}$$

To determine a material's thermal conductivity, Yu and Choi [39] came up with the following new mathematical formula:

$$k_{\mathrm{nf}} = \left[\frac{k_p + 2k_t - 2\varnothing(k_t - k_p)(1+\beta)^3\varnothing}{k_p + 2k_t + \varnothing(k_t - k_p)(1+\beta)^3\varnothing}\right]k_t \tag{4}$$

where β is the ratio of the thickness of the nanolayer to the original particle radius. When calculating the thermal efficiency of a nanofluid, the value $b = 0.1$ is often used. In order to calculate the thermal conductivity of nanofluids, the concept of the effective medium, which was first presented by Timofeeva et al. [40], is used. The effective medium is defined as follows:

$$k_{\mathrm{nf}} = \left[1 + 3\varnothing\right]k_t \tag{5}$$

The thermal conductivity of a microfluid may be measured theoretically in a number of ways. The viscosity of nanofluids is an important consideration when it comes to their performance. It is the goal of this study to examine how well-known models may predict outcomes, and then compare those predictions to what really took place. To determine the viscosity of fluids that include sphere-shaped nanoparticles, Batchelor [41] advises using a simple equation.

$$\mu_{\mathrm{nf}} = \left(1 + 2.5\varnothing + 6.2\varnothing^2\right)\mu_t \tag{6}$$

The Einstein equation for determining the viscosity of spherical particles of volume is proposed by Drew and Passman [42].

$$\mu_{nf} = \left(1 + 2.5\varnothing\right)\mu_t \tag{7}$$

A simplified mathematical representation of Einstein's equation by Brinkman [43] is as follows:

$$\mu_{nf} = \frac{1}{\left(1-\varnothing\right)^{2.5}}\mu_t \tag{8}$$

Viscosity of nanofluids may be calculated using the model developed by Wang et al. [44].

$$\mu_{nf} = \left(1 + 7.3\varnothing + 123\varnothing^2\right)\mu_t \tag{9}$$

where Ø is the molecule volumetric fixation, μ_{nf} is the consistency of the nanofluid and μ_t is the thickness of the therminol or the base liquid.

3.6. Surface tension and agglomeration in mechanical definition

The molecules change from a gas to a sturdier but still disorganised phase known as a liquid when intermolecular contact surpasses heat excitation. In a compressed state called liquid, particles are pulled to one another. Molecules constrained inside the circumference of a liquid benefit from collisions with all neighbouring molecules. Liquids consequently alter their shape to occupy the shortest space possible. The outermost region of the substance's volume is devoid of energy, starving its molecular constituents. A molecular arrangement on the surface of a liquid has around 1/2*E* less bonding energy than the material as a whole if the combined bonding energy per ingredient is *E*. The energy deficit per unit area is clearly indicated by surface tension, which may be characterised by the energy necessary to raise the size of the surface by one unit. Surface tension is defined as an attraction that is orthogonal to the plane of the surface and directed at the liquid. There are surface tension models that have been empirically tested and are based on experimental data in the literature. One of these mathematical models for water with a boiling point range of 273.6–647.3 K is presented by Argaftik et al. [45]. Zhu et al. [46] suggested an equation [10] based on experimental results showing a linear reduction in surface tension of SiC-alkaline water nanofluids in an ambient temperature range of 292–352 K.

$$\partial = 238.8\left[\frac{647.8 - T}{647.8}\right] \times 1.256 + 1 - 0.657\left[\frac{647.8 - T}{647.8}\right] \tag{10}$$

Brownian motion is employed by microscopic particles as they travel closer to the irregularities that surround them. The creation of an assembly occurs when particles are attracted to one another. The fundamental source of nanofluid destabilisation is gravity-induced settling of nanoparticles, which is exacerbated by agglomeration. The proportion of van der Waals forces present in nanoparticles is greater than that in microparticles. As particle distance increases, the van der Waals energies drop. Aggregation between particles reduces the overall functional thermal conductivity of tiny particles and can induce blockage. The most popular approach for producing stable nanofluids is ultrasonication of nanosuspensions [47]. Previous research [48] investigated the settling of floating particles at low and high suspended particle concentrations. The production of flocs affects the settling velocity at high nanoparticle concentrations, and larger agglomerates settle downwards more quickly. Camenen and van Bang [49] and Lester et al. [50] provided mathematical approaches for estimating the impeded settling function.

Coagulation and settling were quantitatively examined using the Brownian dynamics approach in a recent research by Lee et al. [51]. The influence of the size of the particle, focused attention, and the potential for zeta on stability was explored, and it was discovered that tiny and big particles settle differently. Previous research on the manufacture of nanofluids found that sonication breaks down agglomerates in small suspensions and improves stability. However, several studies determined that excessive sonication had a deleterious influence on nanofluid dispersion behaviour.

By capitalizing on the inherent advantages of the chain droplet method, one can effectively conduct precise measurements of liquid tension on the surface. The method employed in this study involved subjecting various substances such as polymers, the water crystals, and low-molecular-mass compounds to rigorous testing in order to ascertain their respective interfacial forces. Great care must be exercised in this experimental procedure, particularly in guaranteeing the immaculateness of the syringe thread tip.

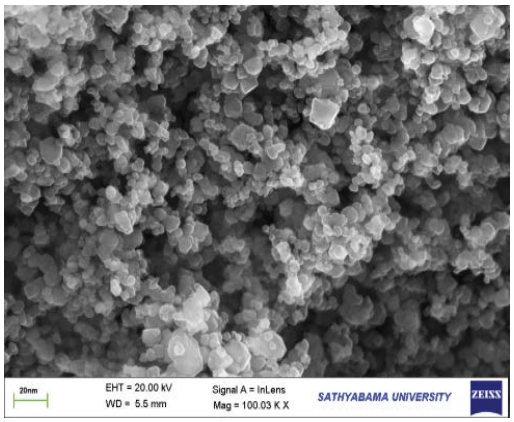

Fig. 4. Scanning electron microscopy SiC.

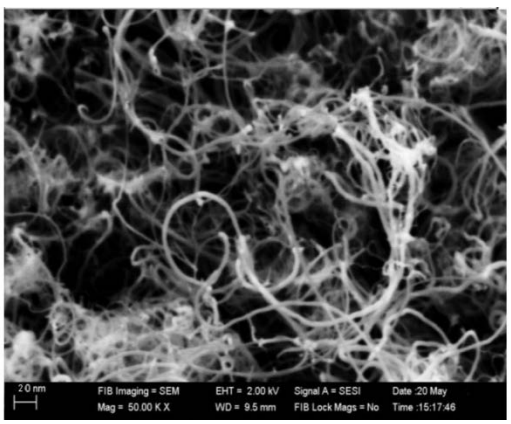

Fig. 5. Scanning electron microscopy ZnO.

When subjected to the influence of contaminants such as fine particles and organic remains like grease, the energy at the tip of the surface experiences a diminishment. In the current series of experiments, the ejection of nanofluids from the syringe at a moderately controlled velocity was undertaken to mitigate the influence of resistance on the observed phenomena. In order to accurately quantify the influence of evaporation, we conducted our experimental observations promptly upon the attainment of the pendent droplet's maximal volumetric capacity, which we have ascertained to be 10 L for highly concentrated solutions. The pressure and surface tension measurements conducted by the FTA200 system are derived from the fundamental principles encapsulated within the Young–Laplace equation [52].

$$\Delta p = \gamma\left(\frac{1}{R_1 + R_2}\right) \tag{11}$$

In the context of interfacial dynamics, Δp represents the pressure differential experienced across a given point on the interface. Meanwhile, R_1 and R_2 denote the respective radii of curvature at said point, as measured from the droplet's profile. The change in momentum, denoted as Δp, can be conveniently determined by observing its relationship with the gravitational force and the disparity in density across the interface. In summary, the phenomenon of nanoparticles adhering to a solid surface leads to a modification of said surface, resulting in the pinning of the contact line to the newly established adsorption sites on the solid surface. In accordance with the principles of molecular kinetics, the advancement of a liquid medium across a solid surface can be understood as a sequential phenomenon wherein liquid molecules successively adhere to specific adsorption sites along the solid surface, following a predetermined direction. Therefore, the sole term that is subject to change in relation to the concentration of nanoparticles is the solid–liquid tension at the interface, as can be seen in Fig. 6.

3.7. Contact angle

The contact angle was quantified through visual analysis of captured images depicting sessile tiny particles of tiny liquids, which were employed in the present investigation. Sessile droplets were experimentally generated on borosilicate glass slides utilizing a casting technique. In the preliminary stage, the nanofluid was expelled from the syringe at an exceedingly modest velocity (e.g., 1 mL/s), and upon encountering the solid substrate, it promptly disengaged from the needle tip. The experimental conditions ensured that the volume of the sessile in nature droplets remained constant at 6 L throughout the duration of the investigation. Henceforth, the immobile droplet manifests a spherical cap, wherein the radius of its corresponding sphere is found to be smaller than the capillary length denoted as CLg =. This observation suggests that the droplet is in a sessile state. The contact angle's magnitude can undergo a significant reduction due to the process of evaporation occurring within the sessile droplet. This reduction is quantified by comparing it to the authentic wetting contact angle. Figs. 7 and 8 illustrate the observed alteration in the state of equilibrium contact angle of nanofluids as a consequence of escalating nanoparticle concentration. Experimental evidence has unequivocally established that the manipulation of nanoparticle concentration yields a discernible augmentation in the state of equilibrium contact angle.

Figs. 7 and 8 exhibit the variation in surface tension of nanofluids with respect to the concentration of nanoparticles. SiC/ZnO – alkaline water nanofluid surface tension and stability angle of contact as a function of nanoparticle concentration shown in Tables 3 and 4. The observed phenomenon reveals a decrease in surface tension as the

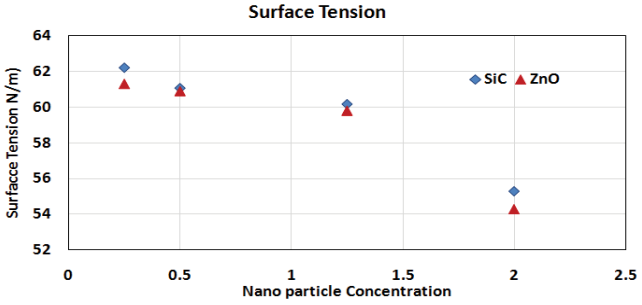

Fig. 6. SiC/ZnO-alkaline water nanofluids exhibit surface tension fluctuation with nanoparticle vol. proportion.

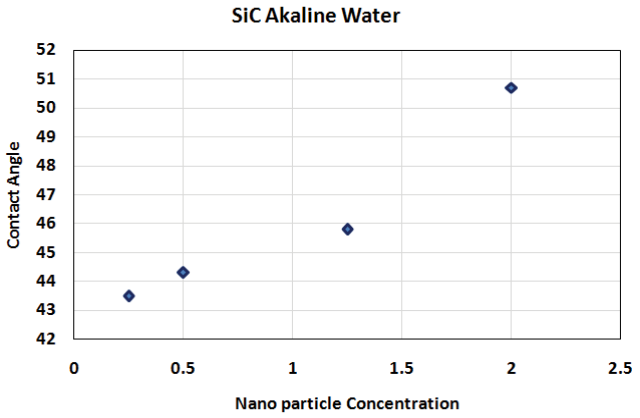

Fig. 7. SiC equilibrium contact angle fluctuation in alkaline water nanofluids with nanoparticle vol. proportion.

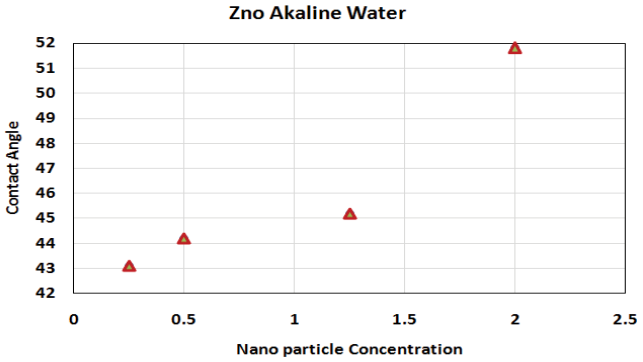

Fig. 8. ZnO equilibrium contact angle fluctuation in alkaline water nanofluids with nanoparticle vol. proportion.

Table 3
Variation in SLγ with respect to SiC-alkaline water nanoparticles concentration

Nanoparticle concentration	Surface tension (mN/m)	Contact angle	$\gamma_{SV}-\gamma_{SL}=\gamma_{LV}\cos\theta$
0.25	62.2	43.5	45.2
0.5	61.1	44.3	43.5
1.25	60.2	45.8	42.7
2	55.3	50.7	40.6

Table 4
Variation in SLγ with respect to ZnO-alkaline water nanoparticles concentration

Nanoparticle concentration	Surface tension (mN/m)	Contact angle	$\gamma_{SV}-\gamma_{SL}=\gamma_{LV}\cos\theta$
0.25	61.3	43.1	44.8
0.5	60.9	44.2	43.9
1.25	59.8	45.2	43.1
2	54.3	51.8	42.9

concentration increases, exhibiting a discernible discrepancy of 8.9 mN/m between the outermost tension of the solution with a lower concentration (0.5% vol.) and the show up tension of the solution with a higher concentration (2% vol.). Moreover, the surface tension of pristine alkaline water has been quantified at 72.8 mN/m, exhibiting an increment of 9.6 mN/m when compared to nanofluids comprising a volumetric concentration of 0.5%. Experimental evidence has unequivocally established a profound correlation between the cohesive energy and the surface tension of the substance under investigation. Upon the introduction of nano-scale particles into the underlying liquid medium, a discernible reduction in the cohesive energy is observed at the interface between said liquid and the surrounding air phase. The observed phenomenon of surface tension reduction in nanofluids is hypothesized to be associated with the aforementioned alteration. Indeed, it is worth noting that the phenomenon under consideration is intricately linked to the intricate Brown's principle that nanoparticles undergo while being immersed within a fluid medium. The phenomenon of Brownian motion exhibits the remarkable capability to induce a reconfiguration of nanoparticles, presently positioned at the interface separating a liquid medium and the surrounding air, into a novel orientation characterized by a diminished aggregate free energy of said interface. Due to the observed phenomenon, it can be inferred that the surface tension will exhibit a notable reduction. Through meticulous investigations into the intricate realm of surface tension, it has been ascertained that a discernible inverse relationship exists between the concentration of nanoparticles and the phenomenon of surface tension. Due to the phenomenon of Brownian motion, nano-scale particles undergo a process wherein they attain the state of minimum interfacial energy. This reduction in energy can be attributed to the decrease in cohesive energy that takes place specifically at the interface between the liquid and air phases. Furthermore, there exists a hypothesis suggesting that nanoparticles possess the potential to fulfil the function typically attributed to surfactant molecules. The observed phenomenon can be attributed to the inherent property of nanoparticles to effectively diminish surface tension through their absorption at the liquid–gas interface. The experimental observations pertaining to the equilibrium contact angle indicate a positive correlation between the concentration of nanoparticles and the corresponding equilibrium contact angle of the nanofluids. The current hypothesis posits that although the disjoining pressure and its associated excess film interaction energy both play a role in promoting spreading, the determination of the equilibrium shape and contact angle of nanofluid droplets on a solid surface is governed by two separate mechanisms. When particles undergo agglomeration processes in highly concentrated solutions, it is hypothesized that one of the contributing factors is a decrease in the extent of enhanced wetting. This observation can be attributed to the reduced particle density within the wedge film. The adsorption phenomenon pertaining to nanoparticles onto the solid surface manifests as the secondary mechanism, thereby inducing alterations in the solid–liquid interface, alongside the immobilization of the contact line. Both of these mechanisms are observed to exhibit a positive correlation with the state of equilibrium angle of contact for nanofluids characterized by higher concentrations.

4. Experimental data calculation

The results of the experiment may be used in the process of calculating several physical variables, including the base external heat sink, the average convective heat transfer rate (h_{av}), thermal characteristics, the Nusselt number, and pumping power (PP). It is essential to understand that the value of hi indicates the local convective heat transfer coefficient and that this value changes based on where the four thermocouples are located [53,54].

$$h_i=\frac{q^{nwL}/N_C\left(\pi DL+3\pi dl-3\left(\frac{1}{2}+\sqrt{2}\right)\pi d^2\right)}{\left(T_{w_i}-T_m\right)} \tag{12}$$

The integral method may be used to the calculation of a local heat transfer rate, as indicated in the following equation, which allows one to determine the average heat transfer rate, denoted by h_{avg}.

$$h_{avg}=\frac{\sum_{i=1}^{3}\left(\frac{h_i+h_{i+1}}{2}\right)\left(x_{i+1}-x_i\right)}{\sum_{i=1}^{3}\left(x_{i=1}-x_i\right)} \tag{13}$$

q'' is the heat flow, and it is used in the calculation of the convective heat transfer rate.

$$q''=\frac{q}{WL} \tag{14}$$

The temperature of the bottom surface of the heat sink is what is utilized to calculate q, and the equation that may be used to calculate it is as follows:

$$q = \rho_{nf} Q C_{P_{nf}} \left(T_{out} - T_{in}\right) \tag{15}$$

The heat sink's thermal resistance is an essential metric to consider when assessing its thermal performance.

$$R_{th} = \frac{T_{W_{max}} - T_{c,in}}{q} \tag{16}$$

where $T_{c,in}$ is the coolant intake temperature, while $T_{w,max}$ is the heat sink bottom wall temperature. The Nusselt number compares convection and conduction heat transfer.

$$Nu = \frac{h_{avg} D}{K_{nf}} \tag{17}$$

Pumping fluid via channels necessitates the measurement of pressure drop across the channel (P) and volume flow rate (Q), which are used to estimate pumping power.

$$P.P = Q \times \left(P_{out} - P_{in}\right) \tag{18}$$

The hydraulic channel diameter multiplied by the Reynolds number yields the following Reynolds number:

$$Re = \frac{\rho_{nf} VD}{\mu_{nf}} \tag{19}$$

where D_{hyd} is the hydraulic diameter.

5. Uncertainty analysis

Due to the fact that detecting physical quantities like temperature, pressure differential, and volume flow rate always implies some degree of uncertainty in the measurement instruments that are used, it is essential to calculate measurement uncertainties. This is a direct result of the fact that calculating measurement uncertainties is a direct result of the fact that calculating measurement uncertainties is a direct result of the fact that calculating measurement uncertainties. The degree of precision with which physical quantities are measured is the primary contributor to the level of uncertainty found in the reported results. We have determined that the quantity of thermal conductivity that the nanofluid has is 2%, and we have established all of the other thermophysical characteristics to be 1% [47,48]. This was done in order to explain for the lack of experimental data in this specific location. Table 5 presents the degrees of uncertainty that were analyzed. The inherent degree of uncertainty that is associated with the outcomes of the experiment may be determined by applying the following equations to the information that is shown in Table 3.

Table 5
Uncertainty of measuring quantities

Properties	AW	SiC	ZnO
D_p (nm)	–	20	20
Density (kg/m^3)	990	3,500	3,740
C_p (J/kg·K)	410.8	980	810
K (W/m·K)	0.6851	45.35	9.4

6. Discussion of findings

6.1. Effect of the Reynolds number and the volume concentration of nanofluids on the temperature of the heat sink's bottom surface

The temperature of the bottom surface of the heat sink, as well as the temperature of the chip itself, should be kept as low as possible throughout the process of cooling electronic chips in order to fulfill the primary purpose of this procedure, which is to create temperature uniformity throughout the system. This will allow the procedure to fulfill its fundamental purpose, which is to create temperature uniformity throughout the system. The life expectancy of electronic components may be significantly increased by taking precautions to limit the range of temperatures that they are exposed to. The fluctuation in bottom surface temperature of the heat sink vs. Reynolds number is shown in Fig. 9a and b for different volume concentrations of bio-synthesized SiC-alkaline water and ZnO-alkaline water. It is abundantly obvious that the use of nanofluids has a considerable influence on temperature change reduction, particularly in the higher Reynolds number range. This is notably the case in situations when the Reynolds number range is larger. The use of bio-synthesized SiC-alkaline water and ZnO-alkaline water reduces temperature variations by about 1.90°C and 1.60°C, respectively, under conditions in which the volume concentration is 2% and the Reynolds number is 1,060 or 1,092, respectively. Temperature shifts, on the other hand, are brought about by the use of alkaline water. As can be shown, elevating the total number of nanoparticles present in the fluid results in a significant acceleration of the pace at which heat is transferred. When nanofluids are utilized, this is the essential component that brings about a decrease in the temperature variance that occurs inside the heat sink.

6.2. Convection heat transfer coefficient of nanofluids

The average heat transfer coefficient of bio-synthesized SiC-alkaline water and ZnO-alkaline water with particles of 20 and 10 nm is shown in Fig. 10a and b, respectively, in relation to the Reynolds number over a range of volume concentrations. The formation of these nanofluids was accomplished by mixing SiC-alkaline water and ZnO-alkaline water. As can be seen in Fig. 7, raising either the volume concentration of nanoparticles or the Reynolds number leads to an increase in the average heat transfer coefficient. The fact that the values of the average heat transfer coefficient for nanofluids are greater than those of pure water should not come as much of a surprise given that these discrepancies are anticipated to be the case. These findings are fairly reasonable. Many different processes, all of which have been recognized as potential contributors to this phenomena, may be responsible for the acceleration in the rate of heat transfer that occurs in nanofluids. This phenomenon has been seen in a number of different contexts. Enhancement of heat conductivity is one of these processes; others include Brownian motion, thermophoresis, and diffusion phoresies. When compared to deionized water, SiC-alkaline water and

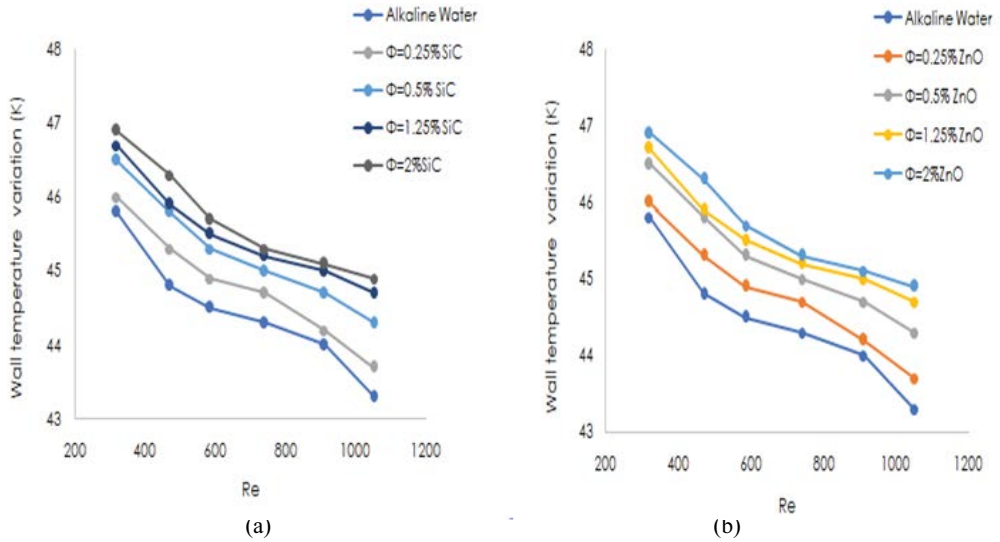

Fig. 9. Influence of Reynolds number and volume concentration of nanofluids on the temperature of the bottom of the heat sink: (a) SiC-alkaline water and (b) ZnO-alkaline water nanofluids.

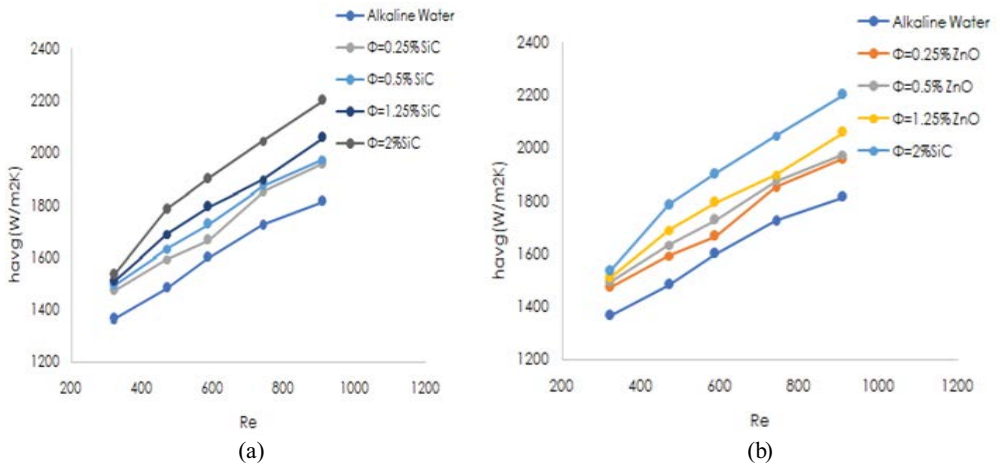

Fig. 10. Effect of nanofluid volumetric concentration and Reynolds number on the convective heat transfer coefficient of the heat sink: (a) SiC-alkaline water and (b) ZnO-alkaline water nanofluids.

ZnO-alkaline water show a maximum increase in the convective heat transfer coefficient of approximately 18% and 16%, respectively, for a volume percentage of 2%. This is in comparison to the fact that deionized water does not contain any dissolved solids. The absence of ions in deionized water stands in stark contrast to this reality. There is a connection between these two types of nanofluids due to the fact that both of them include nanoparticles that are suspended in alkaline water. Fig. 7 demonstrates that when the Reynolds number is increased from 312 to 753, and from 249 to 573, respectively, the slopes of the heat transfer coefficient for SiC-alkaline water and ZnO-alkaline water significantly increase.

As a function of the Reynolds number, the average convective heat transfer coefficient for SiC-alkaline water and ZnO-alkaline water is illustrated in Fig. 11. It has been shown that the coefficient of convective heat transfer between SiC and alkaline water is 2% higher than that between ZnO and alkaline water. It's possible that the higher heat conductivity of SiC-alkaline water is to blame for this disparity, and it's a strong possibility.

6.3. Reynolds number and nanofluid concentration impact Nusselt number

Because the heat transfer coefficient is a function of both the properties of the fluid and the features of the flow, increasing the convective heat transfer coefficient may be accomplished by switching from boundary layer flow to turbulent flow while maintaining the same fluid parameters. The fluctuation of the average Nusselt number against the Reynold number is shown in Fig. 12a and b, respectively, for different volume concentrations of SiC-alkaline water and ZnO-alkaline water. According to the data shown in Fig. 11,

a volume concentration of 2% results in an increase of 12.5% points in the Nusselt number for SiC-alkaline water and 11.6% for ZnO-alkaline water. As can be shown in Fig. 11, the Nusselt quantity for SiC-alkaline water is 0.9% higher than the Nusselt number for ZnO-alkaline water. Because pins are present, the channel of the heat sink transitions from having a laminar flow regime to having a turbulent flow regime. This results in an increase in the convective efficiency of the liquid that is being cooled. As a direct result of the rise in the Nusselt number that was brought about by the use of nanofluids, traditional coolants have been phased out and replaced with nanofluids.

The previously described correlation was discovered by performing a curve fitting operation on all of the experimental data involving SiC-alkaline water and ZnO-alkaline water. The results of this operation revealed the existence of the correlation. The purpose of doing this was to investigate the connection that exists between the two nanofluids. Fig. 13a and b show, respectively, the variation of the experimental Nusselt number compared with the expected value and the volatility of the predicted Nusselt number as shown by correlations. The findings demonstrate that the data obtained via experimentation and the data that were anticipated by the postulated correlations are, to a significant extent, congruent with one another. The fact that both groups of data are in agreement with one another is evidence that this is the case. The amount of inaccuracy that was discovered to be the most significant in the data that was anticipated is roughly in the region of 64%. With the help of these equations, it is possible to make a prediction about the Nusselt number of nanofluids with volume concentrations in the range of 0.25%–2.0% and Reynolds numbers in the range of 298–1,090. This range of volume concentrations and Reynolds numbers is necessary for the prediction to be accurate.

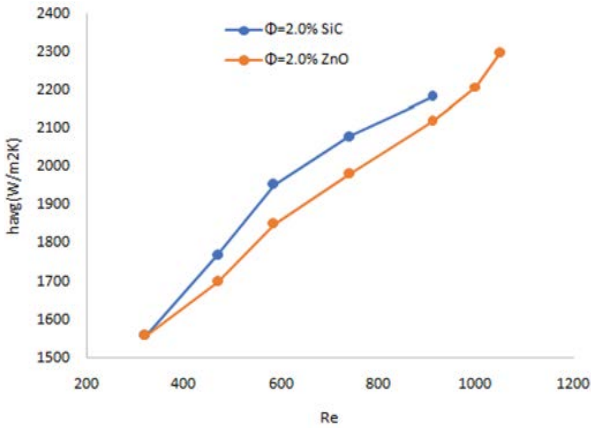

Fig. 11. Average convective heat transfer coefficient vs. Reynolds number for convective heat transfer (a) SiC-alkaline water and (b) ZnO-alkaline water nanofluids.

6.4. Thermal resistance

Fig. 14 illustrates the amount of heat resistance shown by SiC-alkaline water and ZnO-alkaline water with volume concentrations that range from 205 to 1,200. The Reynolds number may take on a variety of different values, with the range going all the way from 205 to 1,200. This figure demonstrates that the thermal resistance decreases as the Reynolds number increases, and it also demonstrates that increasing the volume concentration leads in a decrease in convective thermal resistance when compared to pure distilled water. Both of these findings can be seen by examining the relationship between the Reynolds number and the thermal resistance. When these two statistics are compared to one another, both of these findings become readily apparent.

The primary logic for this change is that increasing the volume concentration results in a reduction in the convective heat resistance of the material. This shift is caused by an increase in the convective heat transfer coefficient of the nanofluid, in addition to an increase in thermal dispersion.

According to the results of this research, the convective thermal resistance of SiC-alkaline water and ZnO-alkaline water was lower when compared to the convective thermal resistance of pure distilled water when the volume concentration and Reynolds number were increased to their maximum values. This drop was 10% and 14%, respectively, lower than the convective thermal resistance of distilled

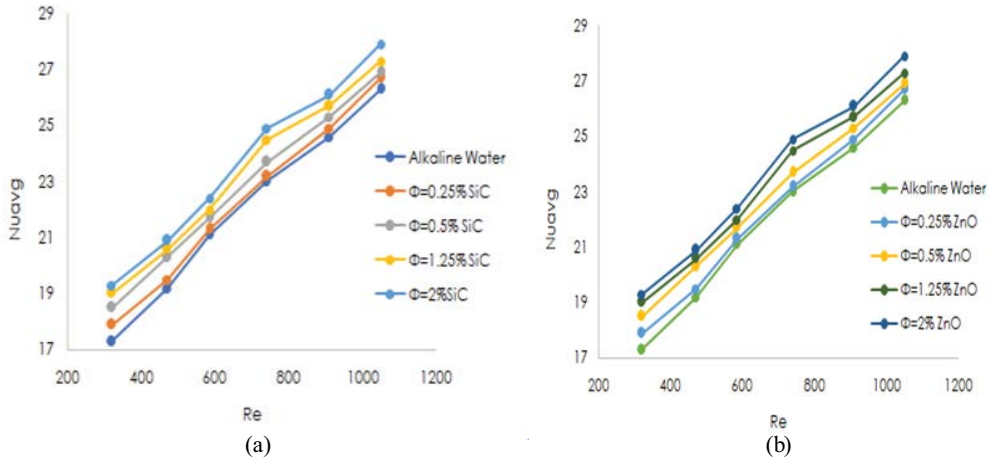

Fig. 12. Effect of nanofluid concentration and Reynolds number on the Nusselt number: (a) SiC-alkaline water and (b) ZnO-alkaline water nanofluids.

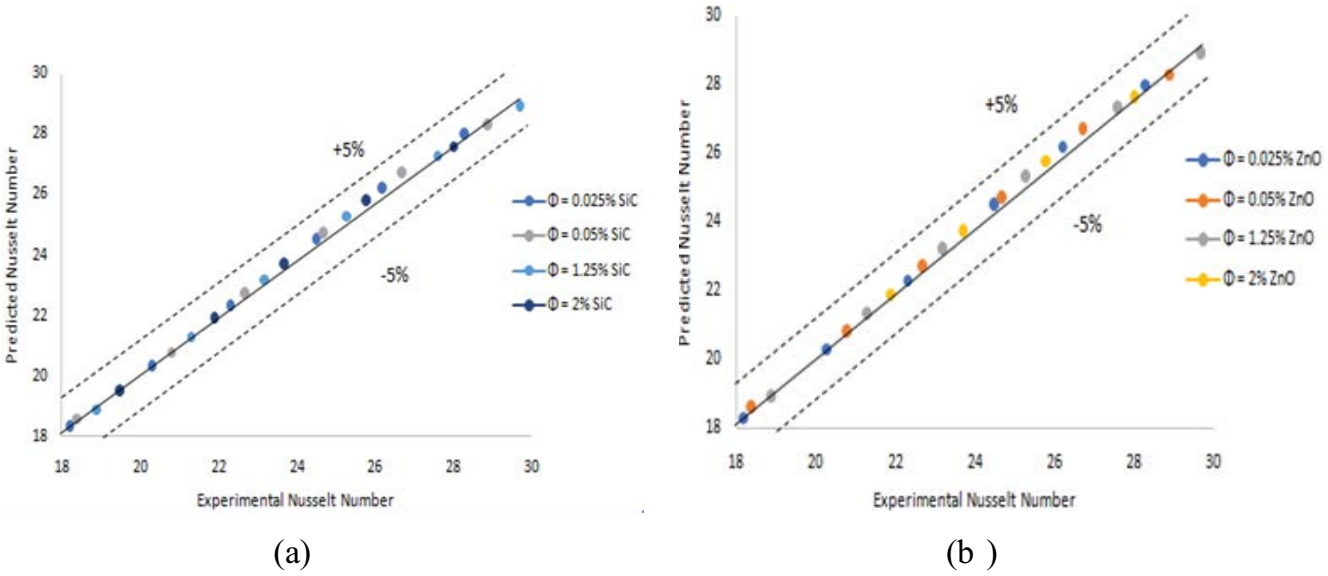

Fig. 13. Experimental Nusselt number vs. theoretical value of the Nusselt statistic for: (a) SiC-alkaline water and (b) ZnO-alkaline water nanofluids.

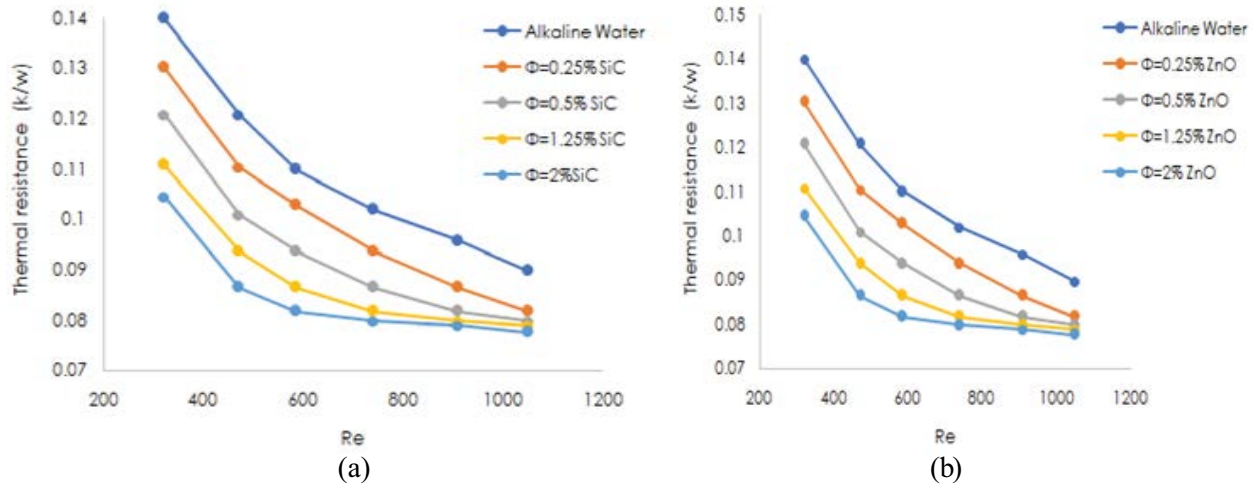

Fig. 14. Impact of nanofluid Reynolds number and volumetric concentration on thermal resistance: (a) SiC-alkaline water and (b) ZnO-alkaline water nanofluids.

water that was completely untouched. Both SiC-alkaline water and ZnO-alkaline water were dissolved in water for the purpose of making a comparison between the two different types of material. Increasing the Reynolds number is necessary in order to achieve the desired effect of enhancing the Brownian motion of nanoparticles. Because of this, a larger degree of heat transfer is experienced by the nanofluid as a direct result of what has just been said. Because of the modifications to the heat transfer, the base temperature of the heat sink drops, and the convective thermal resistance of the heat sink also decreases as a result of these modifications. According to a study that examined the thermal resistances of the two materials, the thermal resistance of SiC-alkaline water is less than 3% lower than the thermal resistance of ZnO-alkaline water. The research was conducted to compare the thermal resistances of the two materials. There is a difference of less than 3% between the thermal resistance of SiC-alkaline water and the thermal resistance of ZnO-alkaline water.

6.5. Pumping power

There is a decrease in tension at the heat sink, which is due to the infusion of fluid from the peripheral edge of the heat drain into the passageway that passes through the heat sink. This is due to the channel flowing through the heat sink. This is as a result of the fact that the channel is located inside the heat sink itself. In order to bring the temperature of the heat sink down, this step is taken. As a direct consequence of this, an increased amount of pumping effort is

necessary in order to make up for the decrease in pressure. The sentence that came before this one has a direct impact on this one. Fig. 12a and b show how the necessary pumping power varies as a function of the Reynolds number for various volume concentrations of SiC-alkaline water and ZnO-alkaline water nanofluids, respectively. Both of these nanofluids are classified as nanofluids in their own right. Both Fig. 12a and b make it abundantly evident that there is a correlation between a rise in pumping power and a subsequent rise in the Reynolds number.

The link between an increase in volume percent and a rise in the Reynolds number, which leads to an increase in pumping power, is seen in Fig. 15. Because the incorporation of nanoparticles into a water-based fluid results in an increase in that fluid's density, nanofluids possess more pumping power than water that has been distilled until it has reached its purest form. This rise in density is brought about by the nanoparticles. The ability of nanofluid to pump is far superior than that of water that has been distilled until it reaches its cleanest possible form. The creation of a nanolayer cluster around the nanoparticle and the improved nanofluid viscosity generated by surface absorption are two additional aspects that contribute to the increase in pumping power. Both of these processes are caused by surface absorption. Both of these effects may be attributed, at least in part, to the absorption that takes place near the surface. When compared to the amount of pumping power necessary for pure distilled water, the outcomes of the research demonstrate that the amount of pumping power required for SiC-alkaline water and ZnO-alkaline water is raised by 35% and 45%, respectively. If you use a nanofluid rather than alkaline water in its purest form, you could see improved thermal performance. This might be enough to make up for the additional pumping power that would be required if you didn't use the nanofluid.

Fig. 16 depicts the connection that exists between the pumping power of SiC-alkaline water nanofluids and the Reynolds numbers of ZnO-alkaline water nanofluids. Both nanofluids are made up of SiC and alkaline water. If the volume concentration remains the same during the experiment, both SiC and ZnO nanofluids will experience an increase in pumping power in response to a rise in the fluid's Reynolds number. This is true even if the experiment is conducted for an extended period of time. Even if there is just a 2% concentration in the volume, this is still the case. When the Reynolds number is maintained constant, the Eckert equation and the Darcy relative roughness demonstrates that the pumping force correlates to viscous and frequency squared, and inversely linked to the density of the fluid. This occurs when the equation and the friction factor are applied to laminar flow. This is the case even when the density of the fluid is maintained at the same level. This relationship continues to exist despite the fact that the Reynolds number that is being used is the same as

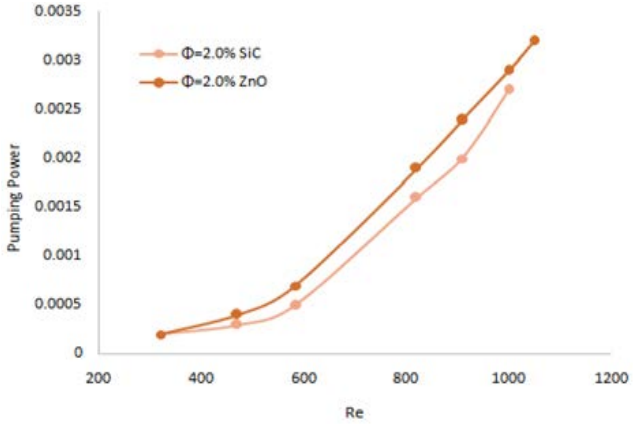

Fig. 16. Correlation between pumping power and Reynolds number for (a) SiC-alkaline water and (b) ZnO-alkaline water nanofluids.

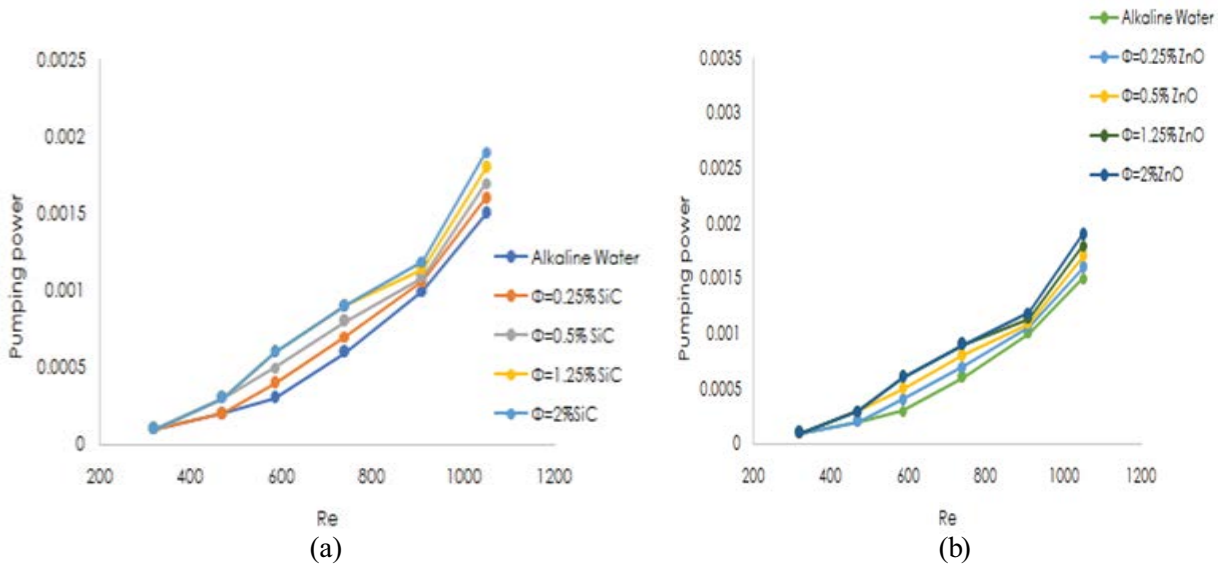

Fig. 15. Effect of pumping power on pumping rate as a function of the Reynolds number and the volumetric concentration of nanofluids: (a) SiC-alkaline water and (b) ZnO-alkaline water nanofluids.

Table 6
Thermal performance comparisons of the current experimental research

Parameters	Present study	Present study	Selvakumar and Suresh [55]
Nanofluid	SiC – AW	ZnO – AW	CuO-H_2O
Volume fraction	0.5%–2.0%	0.5%–2.0%	0.1–0.2
Heat sink dimension (mm)	42 42 14	42 42 14	55 55 19
Width of the channel (mm)	6.0	6.0	0.3
Height of the channel (mm)	10.0	10.0	2
Length of the channel (mm)	42.0	42.0	28
Number of the channel	5	5	49
Flow rate (min^{-1})	0.37–1.5	0.37–1.9	0.79–2.45
Heat input (W)	220.5	220.5	102
Heat transfer coefficient variation	1,463–2,105 for $\varphi = 0.5\%$	1,436–2,159 for $\varphi = 0.5\%$	1,500–1,920 for $\varphi = 0.2\%$
Maximum base temperature reduction (°C)	1.8	1.4	1.15
Pumping power increment	15.0%	30%	15.11%

before. Because this is still the case, it makes no difference whether the Reynolds number that is used is the same or not. Neither option affects the outcome. When compared head to head, the SiC-alkaline water nanofluid has a viscosity that is much greater than that of the ZnO-alkaline water nanofluid. Due to the fact that this is the case, the amount of pumping power that is necessary for the ZnO-alkaline water nanofluid is much less than the amount of pumping power that is necessary for the SiC-alkaline water nanofluid. Because a decrease in the temperature of the working fluid causes a decrease in the viscosity of the working fluid, and the viscosity of the working fluid increases exponentially when the temperature decreases, it is obvious that an increase in the Reynolds number induces a drop in the temperature of the working fluid. This is due to the fact that the permeability of the fluid of operation grows exponentially as temperatures drop. When the Reynolds number of the nanofluids is increased, it becomes more apparent that there is a significant difference in the pumping power of SiC-alkaline water nanofluids and ZnO-alkaline water nanofluids. This is the case because SiC-alkaline water nanofluids are composed of silicon carbide and alkaline water.

6.6. Comparative performance

To contrast and compare the present experimental study with Selvakumar and Suresh's [55] earlier research shown in Table 6, because the geometrical characteristics of the heat sinks varied while the trials were being conducted, the research findings were inconsistent. This study was different from the previous one in that it featured a faster flow rate, a narrower channel, and more apertures. When compared to the present research, a prior one may have had a lower heat transfer coefficient because of a greater heat flow, a higher nanofluid volume concentration, and a higher heat sink base plate reducing temperature. Any one of these factors might be to blame for the decline. In this examination, a much higher heat transfer coefficient was found than in the prior study. The pressure steadily decreased during the research, consistently falling below what was anticipated. By evaluating the rise in the proportion of nanofluids to total volume, this phenomenon may be explained. According to the research, heat transfer coefficients often climb along with rising Reynolds numbers. The nanofluids used, their volume concentrations, their geometrical dimensions, and their flow properties are only a few of the many factors that might be to blame for the differences in results.

7. Conclusion

The thermodynamic and hydraulic efficacy of a PPFHS with slots that are rectangular and elliptic inserts was investigated experimentally. Using base fluids with Reynolds numbers ranging from 300 to 1,100, the heat transmission properties of the two nanofluids were investigated. They were created using nanofluids at 0.25%, 0.5%, 1.25%, and 2% concentrations. When there is turbulence, the average heat transfer coefficient increases. The inclusion of nanofluids improved the thermal performance of pin-fin heat sinks by minimizing variations in wall temperature and increasing cooling efficiency through an improved heat transfer coefficient. The results of the experiment might lead to the following conclusion:

- The adoption of SiC-alkaline water and ZnO-alkaline water nanofluids resulted in temperature drops of 1.08°C and 1.04°C at the heat sink's bottom, respectively.
- When compared to alkaline water, the convective heat transfer coefficient of nanofluids containing 2% volume concentrations of SiC-alkaline water and ZnO-alkaline water rose by 16% and 14%, respectively, over that of alkaline water. It is possible to get a higher Nusselt number by simultaneously raising the volume concentration and the Reynolds number.
- Pumping powers of 1.65×10^{-3} w and 1.77×10^{-3} w were found for ZnO-alkaline water and SiC-alkaline water nanofluids, respectively.
- It has been claimed that pumping power may be enhanced by 30% and 45%, respectively, with the use of solutions containing ZnO-alkaline water and SiC-alkaline water at a volume concentration of 2%. When compared to alkaline water, functioning nanofluids tend to have

greater densities and viscosities, which may be responsible for the improvement in performance.

- The tangential heat sink's heat transfer coefficient is 131% higher than the traditional heat sink's heat transfer coefficient at a Reynolds number of 1,100.
- If you use SiC-alkaline water or ZnO-alkaline water on the bottom of the heat sink rather than pure distilled water, you can bring the average temperature down by 2.28°C and 1.68°C, respectively. In addition to this, thermal uniformity is provided at the base of the heat sink by nanofluids.
- At a Reynolds number of 1,100, the thermal resistance of nanofluids composed of SiC and alkaline water and ZnO and alkaline water with a volume concentration of 2% is reduced by 17% and 14%, respectively.
- It has been claimed that using SiC-alkaline water and ZnO-alkaline water with a volume concentration of 2% may boost consumption pumping power by 30% and 45%, respectively. Both of these solutions are alkaline with a volume concentration. The density and viscosity of working nanofluids increase when compared to water that has been distilled to its purest form, which results in an improvement in both performance and efficiency.

Finally, taking into consideration the obtained experimental findings, it is recommended that the jet impinging approach be used in conjunction with SiC-alkaline water and ZnO-alkaline water nanofluids in the heat sink suggested for pure distilled water for cooling of electronic parts with high heat flux.

Data availability statement

The data that support the conclusions of this research are confirmed to be accessible inside the paper by the authors of the study.

Acknowledgments

The Sathyabama Institute of Science and Technology provided financial assistance for this project. The authors would like to express their gratitude to Centre of Research for providing financial support.

Conflicts of interest

The authors state that there is no potential bias in their work.

Author contributions

Conceptualization, Anish M., Methodology, Rajangam V., software, Ashok Kumar R.; formal analysis, investigation, Anbuchezhian N., data curation, Anish M.; writing—original draft preparation, Anish M.; writing—review and editing, Anish M., visualization, Renugadevi P K., supervision, Anish M., project administration., Anish M.

Funding

This research received no specific grant from any funding agency in the public, commercial, or not-for-profit sectors.

Symbols

A	—	Area, m^2
C_p	—	Heat capacity, J/kg·K
d_p	—	Particle diameter, m
D_{hyd}	—	Hydraulic diameter, m
f	—	Function
h	—	Heat transfer coefficient, $W/m^2·K$
H	—	Height, m
H_{ch}	—	Height of channel, m
k	—	Thermal conductivity, W/m·K
L	—	Length, m
n	—	Shape factor
N	—	Number of pins
N_{ch}	—	Number of channels
N_u	—	Nusselt number
P	—	Perimeter, m
P:P	—	Pumping power, W
D_p	—	Differential pressure, Pa

References

[1] A. Mariadhas, I. Raja, R. Kavvampally, J. Jayaraman, N. Joy, Characteristics of heat transfer and pressure drop in a corrugated plate heat exchanger with chemically synthesized ZnO/sparkling water nanofluids, Desal. Water Treat., 262 (2022) 14–26.

[2] K. Ishida, H. Sakai, Effects of advanced ultraviolet/H_2O_2 treatment on oxidation of linear alkylbenzene sulfonate in detergent wastewater, Desal. Water Treat., 289 (2023) 191–196.

[3] N.R. Kuppusamy, H.A. Mohammed, C.W. Lim, Numerical investigation of trapezoidal grooved microchannel heat sink using nanofluids, Thermochim. Acta, 573 (2013) 39–56.

[4] H.A. Mohammed, G. Bhaskaran, N.H. Shuaib, R. Saidur, Heat transfer and fluid flow characteristics in microchannels heat exchanger using nanofluids: a review, Renewable Sustainable Energy Rev., 15 (2011) 1502–1512.

[5] B.H. Salman, H.A. Mohammed, K.M. Munisamy, A. Sh. Kherbeet, Characteristics of heat transfer and fluid flow in microtube and microchannel using conventional fluids and nanofluids: a review, Renewable Sustainable Energy Rev., 28 (2013) 848–880.

[6] L. Godson, B. Raja, D. Mohan Lal, S. Wongwises, Enhancement of heat transfer using nanofluids—an overview, Renewable Sustainable Energy Rev., 14 (2010) 629–641.

[7] B.H. Salman, H.A. Mohammed, A. Sh. Kherbeet, Heat transfer enhancement of nanofluids flow in microtube with constant heat flux, Int. Commun. Heat Mass Transfer, 39 (2012) 1195–1204.

[8] O. Maťátková, J. Michailidu, A. Miškovská, I. Kolouchová, J. Masák, A. Čejková, Antimicrobial properties and applications of metal nanoparticles biosynthesized by green methods, Biotechnol. Adv., 58 (2022) 107905, doi: 10.1016/j.biotechadv.2022.107905.

[9] M. Chandra Sekhara Reddy, V. Vasudeva Rao, Experimental studies on thermal conductivity of blends of ethylene glycol-water-based TiO_2 nanofluids, Int. Commun. Heat Mass Transfer, 46 (2013) 31–36.

[10] T. Yiamsawasd, A.S. Dalkilic, S. Wongwises, Measurement of the thermal conductivity of titania and alumina nanofluids, Thermochim. Acta, 545 (2012) 48–56.

[11] P. Keblinski, J.A. Eastman, D.G. Cahill, Nanofluids for thermal transport, Mater. Today, 8 (2005) 36–44.

[12] E. Mat Tokit, M.Z. Yusoff, H.A. Mohammed, Generality of Brownian motion velocity of two phase approach in interrupted microchannel heat sink, Int. Commun. Heat Mass Transfer, 49 (2013) 128–135.

[13] P. Naphon, L. Nakharintr, Heat transfer of nanofluids in the mini-rectangular fin heat sinks, Int. Commun. Heat Mass Transfer, 40 (2013) 25–31.

[14] C.J. Ho, W.C. Chen, An experimental study on thermal performance of Al_2O_3/water nanofluid in a minichannel heat sink, Appl. Therm. Eng., 50 (2013) 516–522.
[15] S.K. Das, N. Putra, P. Thiesen, W. Roetzel, Temperature dependence of thermal conductivity enhancement for nanofluids, ASME J. Heat Transfer, 125 (2003) 567–574.
[16] C.T. Nguyen, G. Roy, C. Gauthier, N. Galanis, Heat transfer enhancement using Al_2O_3-water nanofluid for an electronic liquid cooling system, Appl. Therm. Eng., 27 (2007) 1501–1506.
[17] N.A. Roberts, D.G. Walker, Convective performance of nanofluids in commercial electronics cooling systems, Appl. Therm. Eng., 30 (2010) 2499–2504.
[18] B.P. Whelan, R. Kempers, A.J. Robinson, A liquid-based system for CPU cooling implementing a jet array impingement waterblock and a tube array remote heat exchanger, Appl. Therm. Eng., 39 (2012) 86–94.
[19] A. Ijam, R. Saidur, P. Ganesan, Cooling of minichannel heat sink using nanofluids, Int. Commun. Heat Mass Transfer, 39 (2012) 1188–1194.
[20] J.F. Tullius, Y. Bayazitoglu, Effect of Al_2O_3/H_2O nanofluid on MWNT circular fin structures in a minichannel, Int. J. Heat Mass Transfer, 60 (2013) 523–530.
[21] L. Harish Kumar, S.N. Kazi, H.H. Masjuki, M.N.M. Zubir, A review of recent advances in green nanofluids and their application in thermal systems, Chem. Eng. J., 429 (2022) 132321, doi: 10.1016/j.cej.2021.132321.
[22] X. Yu, J. Feng, Q. Feng, Q. Wang, Development of a plate-pin fin heat sink and its performance comparisons with a plate fin heat sink, Appl. Therm. Eng., 25 (2005) 173–182.
[23] Y.-T. Yang, H.-S. Peng, Investigation of planted pin fins for heat transfer enhancement in plate fin heat sink, Microelectron. Reliab., 49 (2009) 163–169.
[24] E.M. Sparrow, J.W. Ramsey, C.A.C. Altemani, Experiments on in-line pin fin arrays and performance comparisons with staggered arrays, J. Heat Transfer, 102 (1980) 44–50.
[25] D. Soodphakdee, M. Behnia, D.W. Copeland, A comparison of fin geometries for heatsinks in laminar forced convection: part I - round, elliptical, and plate fins in staggered and in-line configurations, Int. J. Microcircuits Electron Packag., 24 (2001) 68–76.
[26] S. Ramalingam, G. Sankaranarayanan, S. Senthil, R.A. Rohith, R. Santosh Kumar, Effect of cerium oxide nanoparticles derived from biosynthesis of *Azadirachta indica* on stability and performance of a research CI engine powered by diesel-lemongrass oil blends, Energy Environ., 34 (2023) 886–908.
[27] K.R.B. Singh, V. Nayak, T. Sarkar, R.P. Singh, Cerium oxide nanoparticles: properties, biosynthesis and biomedical application, RSC Adv., 10 (2020) 27194–27214.
[28] A. Saka, Y. Shifera, L.T. Jule, B. Badassa, N. Nagaprasad, R. Shanmugam, L. Priyanka Dwarampudi, V. Seenivasan, K. Ramaswamy, Biosynthesis of TiO_2 nanoparticles by *Caricaceae* (papaya) shell extracts for antifungal application, Sci. Rep., 12 (2022) 15960, doi: 10.1038/s41598-022-19440-w.
[29] A.A. Kashale, A.S. Rasal, G.P. Kamble, V.H. Ingole, P.K. Dwivedi, S.J. Rajoba, L.D. Jadhav, Y.-C. Ling, J.-Y. Chang, A.V. Ghule, Biosynthesized Co-doped TiO_2 nanoparticles based anode for lithium-ion battery application and investigating the influence of dopant concentrations on its performance, Composites, Part B, 167 (2019) 44–50.
[30] A. Ansari, V.U. Siddiqui, W.U. Rehman, Md. Khursheed Akram, W.A. Siddiqi, A.M. Alosaimi, M.A. Hussein, M. Rafatullah, Green synthesis of TiO_2 nanoparticles using *Acorus calamus* leaf extract and evaluating its photocatalytic and in vitro antimicrobial activity, Catalysts, 12 (2022) 181, doi: 10.3390/catal12020181.
[31] A. Maridhas, V.N. Aravind Kumar, S. Kaushik, P. Bency, J. Jayaprabakar, Thermal performance analysis of a double pipe heat exchanger using biosynthesised silicon carbide and carbon nanotubes, Aust. J. Mech. Eng., (2022) 1–9, doi: 10.1080/14484846.2022.2154308.
[32] M. Roshani, S. Ziaeddin Miry, P. Hanafizadeh, M. Ashjaee, Hydrodynamics and heat transfer characteristics of a miniature plate pin-fin heat sink utilizing Al_2O_3-water and TiO_2-water nanofluids, ASME J. Therm. Sci. Eng. Appl., 7 (2015) 031007, doi: 10.1115/1.4030103.
[33] M. Anbuvannan, M. Ramesh, G. Viruthagiri, N. Shanmugam, N. Kannadasan, *Anisochilus carnosus* leaf extract mediated synthesis of zinc oxide nanoparticles for antibacterial and photocatalytic activities, Mater. Sci. Semicond. Process., 39 (2015) 621–628.
[34] S. Vijayakumar, S. Mahadevan, P. Arulmozhi, S. Sriram, P.K. Praseetha, Green synthesis of zinc oxide nanoparticles using *Atalantia monophylla* leaf extracts: characterization and antimicrobial analysis, Mater. Sci. Semicond. Process., 82 (2018) 39–45.
[35] B. Shahmoradi, M. Pirsaheb, M.A. Pordel, T. Khosravi, R.R. Pawar, S.-M. Lee, Photocatalytic performance of chromium-doped TiO_2 nanoparticles for degradation of Reactive Black 5 under natural sunlight illumination, Desal. Water Treat., 67 (2017) 324–331.
[36] H.S. Kwak, H. Kim, J.M. Hyun, T.-H. Song, Thermal control of electroosmotic flow in a microchannel through temperature-dependent properties, J. Colloid Interface Sci., 335 (2009) 123–129.
[37] R.L. Hamilton, O.K. Crosser, Thermal conductivity of heterogeneous two-component systems, Ind. Eng. Chem. Fundam., 1 (1962) 187–191.
[38] S.M.S. Murshed, K.C. Leong, C. Yang, Enhanced thermal conductivity of TiO_2—water based nanofluids, Int. J. Therm. Sci., 44 (2005) 367–373.
[39] W. Yu, S.U.S. Choi, The role of interfacial layers in the enhanced thermal conductivity of nanofluids: a renovated Hamilton–Crosser model, J. Nanopart. Res., 6 (2004) 355–361.
[40] E.V. Timofeeva, A.N. Gavrilov, J.M. McCloskey, Y.V. Tolmachev, S. Sprunt, L.M. Lopatina, J.V. Selinger, Thermal conductivity and particle agglomeration in alumina nanofluids: experiment and theory, Phys. Rev. E, 76 (2007) 061203, doi: 10.1103/PhysRevE.76.061203.
[41] G.K. Batchelor, The effect of Brownian motion on the bulk stress in a suspension of spherical particles, J. Fluid Mech., 83 (1977) 97–117.
[42] D.A. Drew, S.L. Passman, Theory of Multicomponent Fluids, Springer, New York, NY, 2006.
[43] H.C. Brinkman, The viscosity of concentrated suspensions and solutions, J. Chem. Phys., 20 (1952) 571, doi: 10.1063/1.1700493.
[44] X. Wang, X. Xu, S.U.S. Choi, Thermal conductivity of nanoparticle - fluid mixture, J. Thermophys Heat Transfer, 13 (1999) 474–480.
[45] N.B. Argaftik, B.N. Volkov, L.D. Voljak, International tables of the surface tension of water, J. Phys. Chem. Ref. Data, 12 (1983) 817–820.
[46] D.S. Zhu, S.Y. Wu, N. Wang, Surface tension and viscosity of aluminum oxide nanofluids, AIP Conf. Proc., 1207 (2010) 460–464.
[47] R. Penn, B.J. Ward, L. Strande, M. Maurer, Review of synthetic human faeces and faecal sludge for sanitation and wastewater research, Water Res., 132 (2018) 222–240.
[48] J.T. Radford, S. Sugden, Measurement of faecal sludge in-situ shear strength and density, Water SA, 40 (2014) 183–188.
[49] B. Camenen, D.P. van Bang, Modelling the settling of suspended sediments for concentrations close to the gelling concentration, Cont. Shelf Res., 31 (2011) S106–S116.
[50] D.R. Lester, S.P. Usher, P.J. Scales, Estimation of the hindered settling function $R(\varphi)$ from batch-settling tests, AlChE J., 51 (2005) 1158–1168.
[51] J.-H. Lee, K.S. Hwang, S.P. Jang, B.H. Lee, J.H. Kim, S.U.S. Choi, C.J. Choi, Effective viscosities and thermal conductivities of aqueous nanofluids containing low volume concentrations of Al_2O_3 nanoparticles, Int. J. Heat Mass Transfer, 51 (2008) 2651–2656.
[52] I. Roefs, B. Meulman, J.H.G. Vreeburg, M. Spiller, Centralised, decentralised or hybrid sanitation systems? economic evaluation under urban development uncertainty and phased expansion, Water Res., 109 (2017) 274–286.

[53] K.B. Anoop,T. Sundararajan, S.K. Das, Effect of particle size on the convective heat transfer in nanofluid in the developing region, Int. J. Heat Mass Transfer, 52 (2009) 2189–2195.
[54] M.R. Sohel, S.S. Khaleduzzaman, R. Saidur, A. Hepbasli, M.F.M. Sabri, I.M. Mahbubul, An experimental investigation of heat transfer enhancement of a minichannel heat sink using Al_2O_3–H_2O nanofluid, Int. J. Heat Mass Transfer, 74 (2014) 164–172.
[55] P. Selvakumar, S. Suresh, Convective performance of CuO/water nanofluid in an electronic heat sink, Exp. Therm. Fluid Sci., 40 (2012) 57–63.